

6-1-2022

## Effect of raster angle on mechanical properties of 3D printed short carbon fiber reinforced acrylonitrile butadiene styrene

Skhandesh Srinivasan Ganesh Iyer  
*San Jose State University*

Ozgur Keles  
*San Jose State University, ozgur.keles@sjsu.edu*

Follow this and additional works at: [https://scholarworks.sjsu.edu/faculty\\_rsc](https://scholarworks.sjsu.edu/faculty_rsc)

---

### Recommended Citation

Skhandesh Srinivasan Ganesh Iyer and Ozgur Keles. "Effect of raster angle on mechanical properties of 3D printed short carbon fiber reinforced acrylonitrile butadiene styrene" *Composites Communications* (2022). <https://doi.org/10.1016/j.coco.2022.101163>

This Article is brought to you for free and open access by SJSU ScholarWorks. It has been accepted for inclusion in Faculty Research, Scholarly, and Creative Activity by an authorized administrator of SJSU ScholarWorks. For more information, please contact [scholarworks@sjsu.edu](mailto:scholarworks@sjsu.edu).



# Effect of raster angle on mechanical properties of 3D printed short carbon fiber reinforced acrylonitrile butadiene styrene

Skhandesh Srinivasan Ganesh Iyer<sup>\*</sup>, Ozgur Keles<sup>\*\*</sup>

Department of Chemical and Materials Engineering, San Jose State University, San Jose, CA, 95192, USA

## ARTICLE INFO

### Keywords:

Polymer composites  
Fiber reinforcement  
Additive manufacturing  
Raster angle  
Tensile strength  
Flexural strength  
Fracture toughness

## ABSTRACT

The most common additive manufacturing technique fused filament fabrication (FFF) suffers from inter-bead porosity that reduces mechanical properties. Inter-bead pores follow the raster angle, which causes anisotropic mechanical properties. Yet, the effects of raster angle on the mechanical behavior of short-carbon-fiber-reinforced (SCFR) thermoplastics are unclear. In this study, we performed tensile, flexural, and fracture toughness tests on SCFR acrylonitrile butadiene styrene (ABS). Raster angles of 0°, 15°, 30°, 45°, 60°, 75°, and 90° were investigated. Tensile strength and elastic modulus decreased by 22–35% for a change from 0° to 15°. Flexural strength and modulus were less sensitive to raster angle. Flexural strengths were at least 50% more than tensile strength for the same raster angle. Whereas flexural modulus is at least 15% less than elastic modulus. Fracture toughness showed a non-linear relationship with the raster angle. Maximum fracture toughness was observed at 0° and 60° rasters. Crack deflection was observed as the toughening mechanism.

## 1. Introduction

The most common type of additive manufacturing (AM) technique is fused filament fabrication (FFF), also known as fused deposition modeling (FDM) [1]. During the FFF process a thermoplastic is melted and deposited in layer-by-layer fashion following a user-defined path, known as the toolpath. The FFF process is used for various applications in aerospace, automotive, consumer product industries, but it contains various defects [2]. One of the major defects in FFF is the presence of inter-bead porosity, which is caused primarily due to geometrical constraints of the deposition process from a circular nozzle [3]. The build orientation or raster angle directly impacts mechanical properties due to the inter-bead pores following the extrusion head, resulting in anisotropy [2,4]. Some other processing parameters that affect mechanical behavior are nozzle diameter/temperature, bed temperature, infill pattern, infill density, number of outer shells, and extrusion head speed [5]. To enhance the mechanical properties, commercially available short fiber reinforced polymers are used. One of the most common materials used for FFF is the short-carbon-fiber-reinforced acrylonitrile butadiene styrene (SCFR-ABS) [3]. However, the effects of raster angle on the mechanics of SCFR-ABS are unknown.

Short fiber composites contain hard discontinuous fibers laid either

unidirectionally or randomly inside a polymer matrix. The fracture behavior of a fiber-reinforced composite depends on the length, distribution, and orientation of the discontinuous fibers as well as the bonding between the fiber and the matrix [6]. The sources of failure in fiber reinforced composites are matrix delamination and fiber fracture. Fiber orientation also plays a significant role in the strengthening of the composite. The tensile strength (TS) of short fiber composites can be predicted by the Tsai-Hill equation [7]:

$$TS_c = \left[ \frac{\cos^4(\theta)}{\sigma_l^2} + \cos^2(\theta)\sin^2(\theta) \left( \frac{1}{\tau_m^2} - \frac{1}{\sigma_l^2} \right) + \frac{\sin^4(\theta)}{\sigma_t^2} \right]^{-\frac{1}{2}} \quad 1$$

where,  $TS_c$  is the composite tensile strength,  $\tau_m$  the matrix shear strength,  $\theta$  the fiber misorientation angle,  $\sigma_l$  the longitudinal stress ( $\theta = 0^\circ$ ), and  $\sigma_t$  the transverse stress ( $\theta = 90^\circ$ ).

Raster angle ( $\theta$ ) has been shown to affect the tensile and flexural properties of additively manufactured PLA and ABS [8,9]. For PLA, the tensile strength varied between 44.6 MPa and 19.2 MPa for  $\theta = 0^\circ$  and  $\theta = 90^\circ$  specimens with 0.3 mm layer thickness [8]. The tensile strength of FFFed ABS varied between 19.6 MPa and 12.4 MPa for  $\theta = 0^\circ$  and  $\theta = 90^\circ$  specimens [9]. For SCFR polymers, fiber content impacts the mechanical behavior [10,11]. For example, Ning et al. reported a 21%

<sup>\*</sup> Corresponding author.

<sup>\*\*</sup> Corresponding author.

E-mail address: [skhsri@icloud.com](mailto:skhsri@icloud.com) (S. Srinivasan Ganesh Iyer).

decrease in tensile strength with an increase in fiber wt.% from 5% to 10% for SCFR-ABS [10]. A 24% increase in the Young's modulus (E) with 7.5 wt% SCFR-ABS was also reported [10]. Conversely, Tekinalp et al. found a steadily increasing trend in the tensile strength of CFR-ABS by 83%, 36 MPa for 0 wt% carbon fiber and 66 MPa for 40 wt% fiber [11]. This study also reported a decrease in porosity with the addition of short fibers in ABS [11]. Despite the previous studies conducted on both additively manufactured polymers and polymer composites, this is the first study that explores tensile, flexural, and fracture toughness behavior of SCFR-ABS using the same material and processing parameters.

The effects of the raster angle on the tensile, flexure, and fracture toughness behavior on commercially available composite filaments are unknown, limiting wider use of the material in functional products. For example, there is an increasing number of free, online CAD designs of bike parts, skateboard parts, or other load bearing products. These designs can be printed with sub-optimal properties and risk injury. Commercially reported mechanical property data comes from a 3D printer with factory-level optimized settings and materials that are not easily accessible to the public. In this context, we report the effects of raster angle on the tensile strength, elastic modulus, flexural strength, flexural modulus, and fracture toughness ( $K_{Ic}$ ) of FFFed SCFR-ABS. Fractography was performed on selected samples using scanning electron microscopy.

## 2. Materials and methods

3DXTECH CarbonX carbon fiber ABS filaments were used to print test tensile, flexure, and fracture toughness specimens. Tests were performed following ASTM standards D638 Type I (tensile), D7264 (flexure), and D5045 (fracture toughness) [12–14]. A modified prusa i3 system with a hardened steel nozzle was used to manufacture samples (Fig. 1) with the printing parameters given in Table 1. The reported carbon fiber content is 15 vol %, but previous X-ray computed tomography on the same material showed that fiber content could change along the filament within 6–10 vol % in the extruded beads [3]. The specimens were printed using a rectilinear infill with 100% infill density and 90% outline overlap in an XY orientation. Five specimens per angle for tension and flexure, while three specimens per angle for fracture toughness were tested (Fig. 1).

Tensile and flexural tests were performed at room temperature using an Instron 4204 testing machine at a constant crosshead speed of 5 mm/min. The tensile specimens were printed to a thickness of 3.2 mm. The

**Table 1**  
FFF printing parameters.

Nozzle Diameter (mm)	0.6
Layer Height (mm)	0.35
Print Speed (mm/s)	40
Nozzle Temperature (°C)	235
Bed Temperature (°C)	125
Raster Angle	0°–90°
Infill Pattern	Rectilinear

elastic modulus for all tested specimens were calculated within 0.0–0.2% strain (most linear region). Flexural test specimens were  $128 \times 13 \times 4$  mm in size (Fig. 1).

Single edge notch bend (SENB) fracture toughness testing was performed at room temperature at a constant crosshead speed of 10 mm/min. The notch was printed during the FFF process at a depth of approximately 10 mm from the striking edge. Fresh razor blades were tapped to create the initial crack. Using a Leiza MZ12 stereo microscope, the notch tip radius of the samples was  $0.27 \pm 0.3$  mm and the crack tip radii were less than  $\sim 20$   $\mu$ m, measured from 7 samples. Fracture surfaces were investigated using an FEI Quanta 200 scanning electron microscope (SEM).

## 3. Results and discussion

A decreasing trend in tensile and flexural mechanical properties with increasing raster angle was observed. Specifically, a raster angle change from 0° to 15° caused a large reduction in properties. The effects of raster angle on the tensile strength, elastic modulus, flexural strength, flexural modulus, and fracture toughness of FFFed SCFR-ABS are given in Fig. 2.

### 3.1. Effect of raster angle on tensile strength and elastic modulus

The strongest fiber-reinforced composite is achieved when the fiber axis is parallel to the direction of the applied load (0°). However, tensile strength decreased by 22% from 31.5 MPa to 24.6 MPa for a change in  $\theta$  from 0° to 15° (Fig. 2a). A similar decrease in tensile strength with  $\theta$  is also reported for continuous fiber reinforced nylon [16]. Tensile strength was between 23.0 MPa and 17.1 MPa for  $30^\circ \leq \theta \leq 90^\circ$ . In 0° orientation, fiber fracture is expected, but the consumer-grade SCFR-ABS has carbon fibers shorter than 300  $\mu$ m, which also breaks down and becomes smaller than 100  $\mu$ m when passing through the

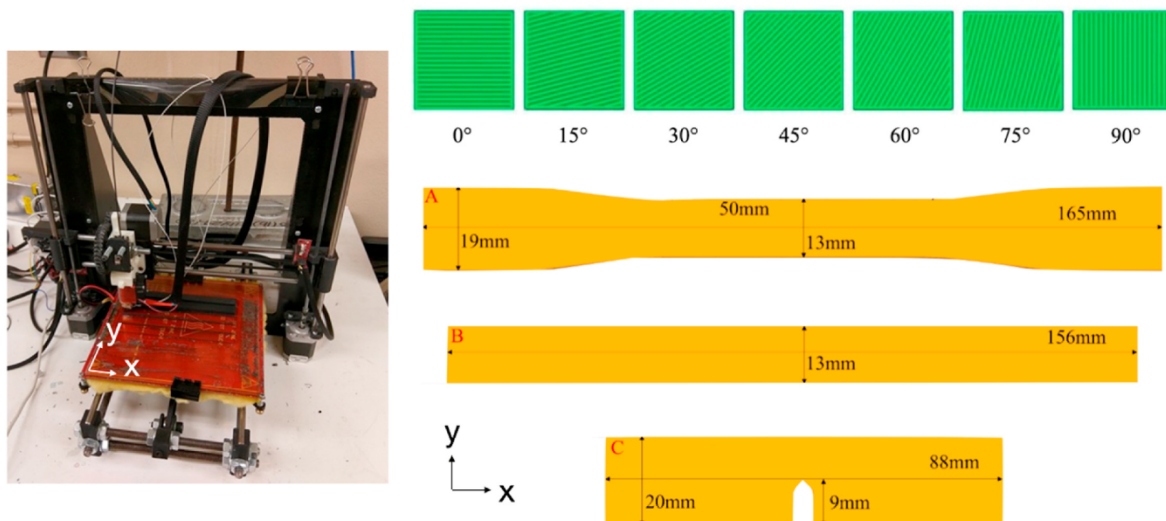


**Fig. 1.** Image of the printer used for manufacturing. Illustration of raster angles and specimen dimensions in XY build orientation for A) tensile, B) flexural, C) fracture toughness tests.

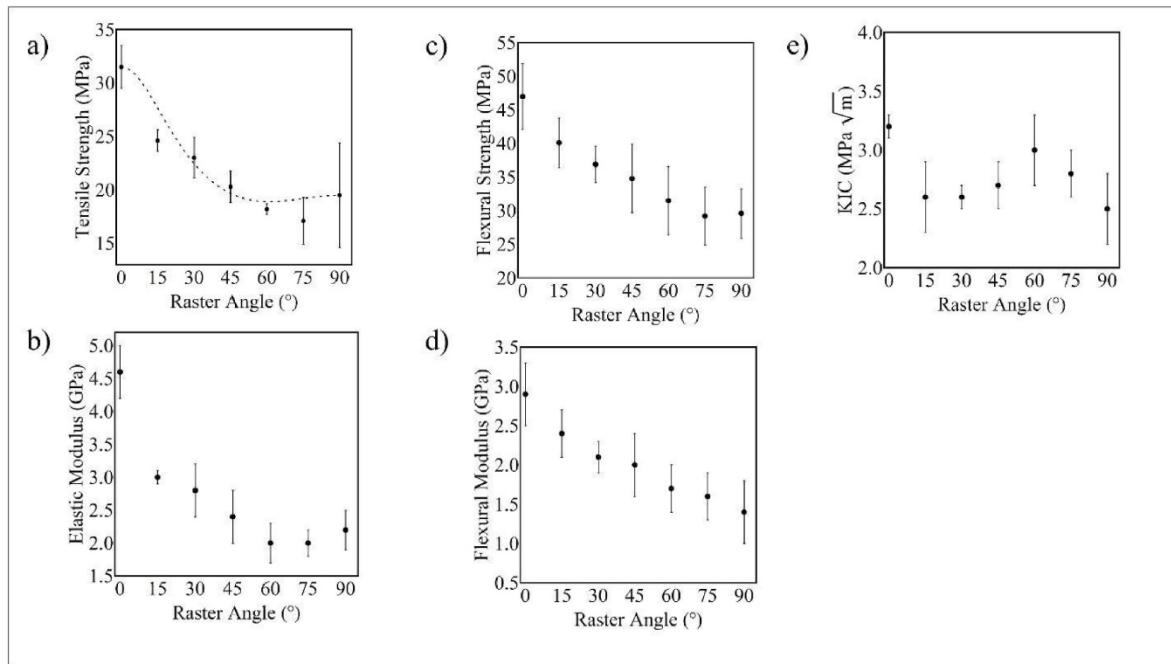


**Fig. 2.** Variation of mechanical properties with raster angle a) tensile strength, b) elastic modulus, c) flexural strength, d) flexural modulus, and e) Mode I fracture toughness.

extrusion nozzle [3]. As a result, the fiber reinforcement is limited. Nonetheless, we used the Tsai-Hill equation (Eq. (1)) to predict the change in tensile strength with the raster angle (dotted line in Fig. 2a), which captured the decreasing tensile strength trend. Experimental strengths at  $0^\circ$  (31.5 MPa) and  $90^\circ$  (19.5 MPa) were used as  $\sigma_l$  and  $\sigma_t$  values, respectively. Using these values Eq. (1) was fitted to the rest of the tensile strength data using the generalized reduced gradient (GRG) method in Excel. The Tsai-Hill fit resulted in a shear strength  $\tau_m$  of 11.2 MPa that matched the experimentally reported shear strength of ABS 11.4 MPa [15]. A noticeable difference was observed at  $15^\circ$ , where the tensile strength is lower than Eq. (1) predicted strength, showing the sub-optimal strengthening in consumer-grade SCFR-ABS. The reason for the deviation from the theoretical predictions at  $15^\circ$  is that not only fiber orientation, but also inter-bead pore orientation changes with raster angle that is not accounted by the failure criterion. The FFF composites, therefore, are expected to have lower strength compared to a pore-free fiber composite in specifically off-axis orientations due to the elongated shape of the inter-bead defects inherent to the FFF process. Here, a Tsai-Hill fit is used to compare the theoretical strength prediction to experimental FFF tensile strengths.

Elastic modulus also decreased by 35% from 4.6 GPa to 3.0 GPa for a change in raster angle of  $0^\circ$ – $15^\circ$  (Fig. 2b). Elastic modulus was between 2.8 GPa and 2.0 GPa for  $30^\circ$  or higher raster angles. The elastic modulus did not show a constant decrease with increasing raster angle. The lowest elastic modulus was  $\sim 2.0$  GPa at  $60^\circ$ , which was increased to  $\sim 2.2$  GPa at  $90^\circ$ . Theoretically, linear elastic models of FFFed ABS elastic modulus show a minimum modulus between  $45^\circ$  and  $60^\circ$  with a model that accounts for inter-bead pores [17]. This behavior is like the observed elastic modulus change with raster angle in Fig. 2b. Note that, the modulus also depends on the inter-bead pore size and shape. For raster angles other than  $0^\circ$  and  $90^\circ$ , there are shear strain contributions to the strain in the tensile direction. Therefore, a minimum modulus is predicted at  $45^\circ$  for low inter-bead porosity FFFed materials [17].

### 3.2. Effect of raster angle on flexural strength and flexural modulus

Flexural strength decreased by 15% from 47.0 MPa to 40.1 MPa for a change in  $\theta$  from  $0^\circ$  to  $15^\circ$  (Fig. 2c). Flexural strength was between 36.9

MPa and 29.2 MPa for  $30^\circ$ – $90^\circ$ . Flexural strength is  $\sim 50\%$  higher than tensile strength at  $0^\circ$ , 63% at  $15^\circ$ , 60% at  $30^\circ$ , 71% at  $45^\circ$ , 73% at  $60^\circ$ , 71% at  $75^\circ$ , and 52% at  $90^\circ$ . Under 3-pt bending, a smaller volume experiences tensile loading at the midpoint, compared to tensile loading. Therefore, the probability of finding larger defects or defect clusters is higher in tensile than in flexural testing, which lowers the tensile strength compared to flexural strength. In addition to the probabilistic explanation for the higher flexural strength, stress concentration around inter-bead pores is lower under bending compared to tensile tests. The layer height is 0.35 mm, which means the inter-bead pore is  $\sim 0.3$  mm away from the highest tensile stresses under bending, reducing the stress concentration. Therefore, higher strengths were observed under bending compared to tensile testing.

Flexural modulus, on the other hand, decreased by 17% from 2.9 GPa to 2.4 GPa for a change in  $\theta$  from  $0^\circ$  to  $15^\circ$  (Fig. 2d). Flexural modulus was between 2.1 GPa and 1.4 GPa for  $30^\circ \leq \theta \leq 90^\circ$ . Compared to elastic modulus, flexural modulus was 37% lower at  $0^\circ$ , 20% at  $15^\circ$ , 25% at  $30^\circ$ , 17% at  $45^\circ$ , 15% at  $60^\circ$ , 20% at  $75^\circ$ , and 36% at  $90^\circ$ . Simulations and classical laminate theory with orthotropic material properties have been shown to predict modulus changes in FFF materials with raster orientation and fiber content [18–20]. Although there is no direct study investigating the effect of raster orientation on the flexural modulus of FFFed SCFR composites, the decreasing load transfer to fibers with increasing raster angle reduces flexural modulus. The effects of inter-bead pore orientation on the flexural modulus are more complex compared to tensile studies because the stress state changes from tensile to compression in bending configuration. Note that, the literature studies do not include any inner-bead porosity for modulus predictions. More numerical investigations are needed on this topic.

### 3.3. Effect of raster angle on fracture toughness

Fracture toughness ( $K_{IC}$ ) decreased by 19% from 3.2 MPa $\sqrt{m}$  to 2.6 MPa $\sqrt{m}$  for a change in  $\theta$  from  $0^\circ$  to  $15^\circ$  (Fig. 2e). This initial decrease was followed by an increase up to 3.0 MPa $\sqrt{m}$  at  $\theta = 60^\circ$ . A further decrease in  $K_{IC}$  was observed at  $75^\circ$  and  $90^\circ$  with lowest  $K_{IC} = 2.5$  MPa $\sqrt{m}$  at  $\theta = 90^\circ$ . The  $0^\circ$  raster has the highest toughness because the crack tip tensile stresses are parallel to the fiber direction, which is the

strongest direction. In addition, inter-bead pores are also parallel to the crack tip stresses (Fig. 3). Whereas the 90° raster has the lowest toughness because the fiber orientation and inter-bead pores are perpendicular to the crack tip stresses. This configuration amplifies the local stresses and reduces toughness (Fig. 3). Toughness at  $\theta = 60^\circ$  was nearly as high as the toughness of 0° raster specimens. The reason for this is the deflection of the crack along the inter-bead pores. Once the crack is oriented away from the highest Mode I tensile stresses, further crack propagation requires higher energy; hence, the higher toughness. Note that the tested composites show nearly linear elastic behavior under tension. Therefore, under plane strain conditions, critical energy release rate ( $G_{IC}$ ) is equal to  $(K_{IC}^2(1-\nu^2))/E$  ( $\nu$  is the Poisson's ratio). The deflected crack paths are shown in Fig. 3. Similar crack deflection was reported for the FFFed SCFR-nylon, where 75° and 60° rasters deflected cracks and had higher mechanical properties compared to  $\theta = 90^\circ$  [21]. The effectiveness of the crack deflection toughening mechanism decreased with  $\theta > 60^\circ$ . Yet, it is a toughening approach that can be modeled to create wavy or zig-zag deposition paths to further enhance toughness of FFFed materials.

Raster angle dictates the orientation of the short fibers and inter-bead pores (Fig. 4 red circles). Depending on the material and FFF parameters, 5–12 vol% inter-bead porosity is common for FFFed parts. A ~15 vol% total porosity with ~5 vol% inner-bead and ~10 vol% is inter-bead porosity was reported for the same material and processing parameters, with details given in Ref. [3]. Briefly, the dimension and weight of the samples were used to calculate the density and total porosity. Inner-bead porosity was subtracted from the total porosity to find the inter-bead porosity. X-ray computed tomography results from Ref. [3] was used for the inner-bead porosity. The main origin of the inner-bead porosity is the inherited porosity from the commercial filament. The as-received filaments have pores in the center that were created during the filament production. Moreover, FFF extrusion heat can create inner-bead pores. Thus, internal porosity and reduced fiber length from broken fibers lower the effectiveness of fiber strengthening. A 20–50% decrease in fiber length was reported for the same system [3]. As a result, commercial SCFR-ABS has lower mechanical properties compared to carefully lab-processed ABS containing longer fibers [9].

Previous studies show that for the same material the average fiber length in the as-received filament is  $132 \pm 70 \mu\text{m}$  which decreases to  $84 \pm 48 \mu\text{m}$  after extrusion [3]. The fiber length was calculated by ImageJ using the optical images of the fibers (~400 fibers) after dissolving SCFR-ABS in acetone [3]. From a critical fiber length  $l_c = (\sigma_f d)/(2\tau)$  point of view, short fiber length should be greater than ~220–570  $\mu\text{m}$  for effective strengthening of ABS [3,22]. For this calculation, we used ABS shear strength ( $\tau$ ) between 15 and 30 MPa, carbon fiber tensile strength ( $\sigma_f$ ) of 2.16 GPa, and fiber diameter ( $d$ ) of 6–8  $\mu\text{m}$ . Note that, short fibers that are ten times the  $l_c$  reaches 95% of the continuous fiber strength [3]. However, extrusion nozzle diameters are 0.4–0.8 mm,

which are easily clogged by the longer fibers. Therefore, FFF of SCFR composites is suitable for big-area manufacturing and larger nozzles, but not for layer heights <0.2 mm. This bottleneck can be overcome by using a tapered nozzle that takes in filament smoothly, avoiding any sharp reduction in diameter that results in clogging and fiber breakage. Moreover, inducing vibrations along the extrusion nozzle and tip can reduce clogging events and reduce inter-bead porosity, ultimately creating stronger and tougher FFF parts [23].

#### 4. Conclusion

We manufactured tensile, flexure, and fracture toughness specimens using commercially available SCFR-ABS and a consumer-grade FFF 3D printer. The effects of raster angle on the mechanical properties were investigated in seven orientations  $\theta$ : 0°, 15°, 30°, 45°, 60°, 75°, and 90°. The experiments show that raster orientation impacts all the mechanical properties due to changes in inter-bead pore orientation. However, the effect of  $\theta$  varies for different mechanical properties. Significant differences between tensile and flexural properties were observed, which indicate processing improvements at the fiber and extrusion scales could increase tensile strength by 50% or more in SCFR-ABS. Based on the experiments, the following conclusions can be made:

1. The change in  $\theta$  from 0° to 15° reduced tensile strength by 22% from 31.5 MPa to 24.6 MPa and reduced elastic modulus by 35% from 4.6 GPa to 3.0 GPa.
2. The change in  $\theta$  from 0° to 15° reduced flexural strength by 15% from 47.0 MPa to 40.1 MPa and reduced flexural modulus by 17% from 2.9 GPa to 2.4 GPa.
3. Flexural strength was at least 50% higher than tensile strength for all the raster angles. Whereas flexural modulus was at least 15% lower than elastic modulus for the same  $\theta$ .
4. Fracture toughness decreased by 19% from 3.2  $\text{MPa}\sqrt{\text{m}}$  to 2.6  $\text{MPa}\sqrt{\text{m}}$  for a change in  $\theta$  from 0° to 15°. The lowest  $K_{IC}$  values of 2.5–2.6  $\text{MPa}\sqrt{\text{m}}$  were observed at 15°, 30°, and 90°. Toughness increased towards  $\theta = 60^\circ$  and reached 3.0  $\text{MPa}\sqrt{\text{m}}$ . Crack deflection is the potential toughening mechanism at this orientation.

#### Funding

The authors are thankful for the partial support by the College of Engineering, San Jose State University.

#### CRediT authorship contribution statement

**Skhandesh Srinivasan Ganesh Iyer:** Conceptualization, Investigation, Methodology, Software, Writing – original draft, Writing – review & editing, Formal analysis, Data curation. **Ozgur Keles:** Resources,

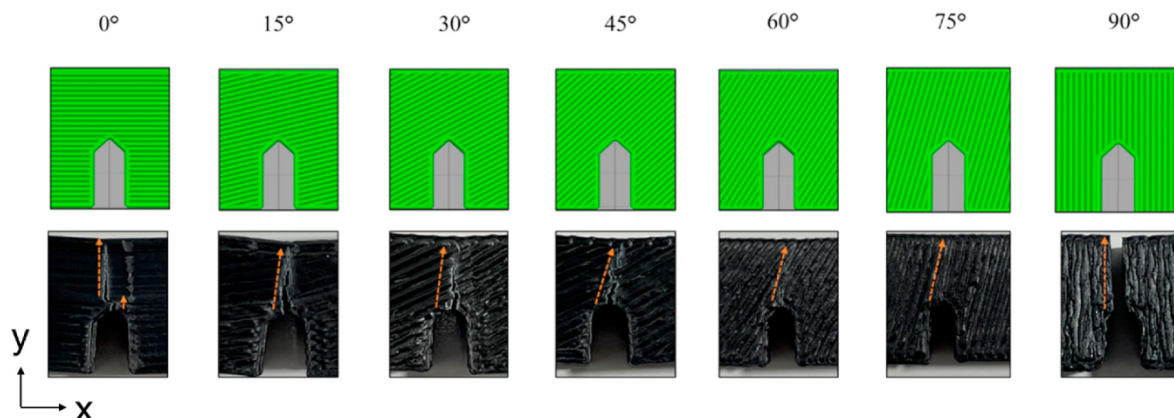
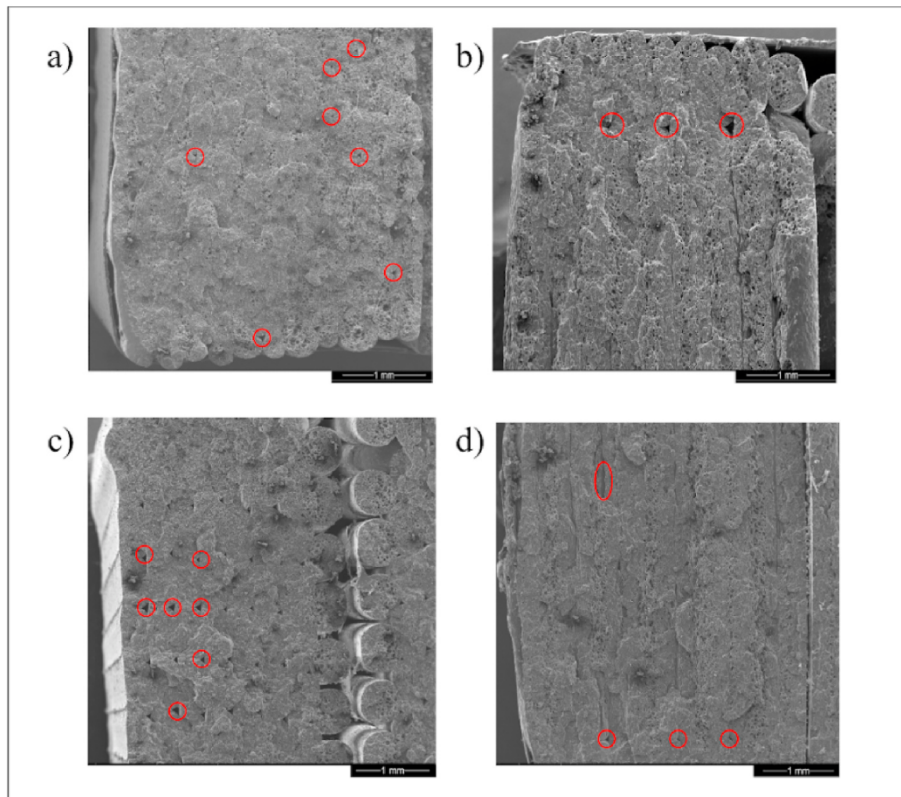


Fig. 3. Illustrations of raster angles and related crack paths in toughness specimens.



**Fig. 4.** Fracture surfaces of the tensile specimens at a)  $\theta = 0^\circ$  and b)  $\theta = 90^\circ$ , and flexural specimens at c)  $\theta = 0^\circ$  and d)  $\theta = 90^\circ$ . Red circles show some of the inter-bead porosity. Scale bars represent 1 mm. (For interpretation of the references to colour in this figure legend, the reader is referred to the Web version of this article.)

Writing – review & editing, Supervision, Formal analysis, Validation, Project administration.

#### Declaration of competing interest

The authors declare that they have no known competing financial interests or personal relationships that could have appeared to influence the work reported in this paper.

#### Acknowledgements

Authors thank Christian Nunez for assisting with 3D printing and mechanical testing.

#### References

- [1] D.W. Gibson, R.B. Stucker, *Additive Manufacturing Technologies, Rapid Prototyping to Direct Digital Manufacturing*, 2009.
- [2] Ö. Keleş, C.W. Blevins, K.J. Bowman, Effect of build orientation on the mechanical reliability of 3D printed ABS, *Rapid Prototyp. J.* 23 (2) (2017), 2017.
- [3] Ö. Keleş, E.H. Anderson, J. Huynh, J. Gelb, J. Freund, A. Karakoç, Stochastic fracture of additively manufactured porous composites, *Sci. Rep.* 8 (1) (2018) 1–2.
- [4] F.M. Afrose, S. Masood, M. Nikzad, P. Iovenitti, Effects of build orientations on tensile properties of PLA material processed by FDM, *Adv. Mater. Res.* 1044–1045 (2014) 31–34.
- [5] D. Popescu, A. Zapciu, C. Amza, F. Baci, R. Marinescu, FDM process parameters influence over the mechanical properties of polymer specimens: a review, *Polym. Test.* 69 (2018) 157–166.
- [6] S. Fu, B. Lauke, Effects of fiber length and fiber orientation distributions on the tensile strength of short-fiber-reinforced polymers, *Compos. Sci. Technol.* 56 (1996) 1179–1190.
- [7] T.H. Courtney, *Mechanical Behavior of Materials*, second ed., Waveland Press, Long Grove, IL, USA, 2000.
- [8] Y. Zhao, Y. Chen, Y. Zhou, Novel mechanical models of tensile strength and elastic property of FDM AM PLA materials: experimental and theoretical analyses, *Mater. Des.* 181 (2019).
- [9] F.R. José, J.P. Thomas, J.E. Renaud, Mechanical behavior of acrylonitrile butadiene styrene (ABS) fused deposition materials. *Experimental investigation*, *Rapid Prototyp. J.* 7 (2001) 148–158.
- [10] F. Ning, W. Cong, J. Qiu, J. Wei, S. Wang, Additive manufacturing of carbon fiber reinforced thermoplastic composites using fused deposition modeling, *Compos. B Eng.* 80 (2015) 369–378.
- [11] H.L. Tekinalp, V. Kunc, G.M. Velez-Garcia, C.E. Duty, L.J. Love, A.K. Naskar, C. A. Blue, S. Ozcan, Highly oriented carbon fiber–polymer composites via additive manufacturing, *Compos. Sci. Technol.* 105 (2014) 144–150.
- [12] ASTM International, ASTM D638-14: Standard Test Method for Tensile Testing of Plastics, 2014.
- [13] ASTM International, ASTM D7264-15: Polymer Composite, Standard Test Method for Flexural Properties of Polymer Matrix Composite Materials, 2015.
- [14] ASTM International, ASTM D5045-14: Standard Test Methods for Plane-Strain Fracture Toughness and Strain Energy Release Rate of Plastic Materials, 2014.
- [15] W. Zhang, A.S. Wu, J. Sun, Z. Quan, B. Gu, B. Sun, C. Cotton, D. Heider, T. Chou, Interfacial bonding strength of short carbon fiber/acrylonitrile-butadiene-styrene composites fabricated by fused deposition modeling, *Composites Part B* 137 (2018) 51–59.
- [16] S.S. Luke, D. Soares, J.V. Marshall, J. Shredden, O. Keles, Effect of fiber content and fiber orientation on mechanical behavior of fused filament fabricated continuous-glass-fiber-reinforced nylon, *Rapid Prototyp. J.* 27 (7) (2021) 1346–1354.
- [17] B. Huang, S. Singamneni, Raster angle mechanics in fused deposition modelling, *J. Compos. Mater.* 49 (3) (2015) 363–383.
- [18] C. Casavola, A. Cazzato, V. Moramarco, C. Pappalettere, Orthotropic mechanical properties of fused deposition modelling parts described by classical laminate theory, *Mater. Des.* 90 (2016) 453–458.
- [19] D. Krzikalla, J. Měsíček, R. Halama, J. Hajnýš, M. Pagáč, T. Čegan, P. Jana, On flexural properties of additive manufactured composites: experimental, and numerical study, *Compos. Sci. Technol.* 218 (2022), 109182.
- [20] J.F. Rodríguez, J.P. Thomas, J.E. Renaud, Mechanical behavior of acrylonitrile butadiene styrene fused deposition materials modeling, *Rapid Prototyp. J.* 9 (4) (2003) 219–230.
- [21] B. Croom, M. Flores, D. Rapking, O. Keles, J. Degery, Prediction of Crack Propagation along Non-uniform Raster Patterns in AM Composites, 2020. Conference: American Society for Composites Conference.
- [22] T. Ohsawa, A. Nakayama, M. Miwa, A. Hasegawa, Temperature dependence of critical fiber length for glass fiber-reinforced thermosetting resins, *J. Appl. Polym. Sci.* 22 (1978) 3203–3212.
- [23] Ö. Keleş, E.H. Anderson, J. Huynh, Mechanical reliability of short carbon fiber reinforced ABS produced via vibration assisted fused deposition modeling, *Rapid Prototyp. J.* 24 (9) (2018) 1572–1578.